

# Mass enhancement, correlations, and strong coupling superconductivity in the $\beta$ -pyrochlore $\text{KO}_{\text{Os}_2}\text{O}_6$

M. Brühwiler,\* S.M. Kazakov, J. Karpinski, and B. Batlogg

*Laboratory for Solid State Physics, ETH Zürich, 8093 Zürich, Switzerland.*

(Dated: September 16, 2018)

## Abstract

To assess electron correlation and electron-phonon coupling in the recently discovered  $\beta$ -pyrochlores  $\text{KO}_{\text{Os}_2}\text{O}_6$  and  $\text{RbOs}_2\text{O}_6$ , we have performed specific heat measurements in magnetic fields up to 14 T. We present data from high quality single crystalline  $\text{KO}_{\text{Os}_2}\text{O}_6$ , showing that  $\text{KO}_{\text{Os}_2}\text{O}_6$  is a strong coupling superconductor with a coupling parameter  $\lambda_{\text{ep}} \approx 1.0$  to 1.6 ( $\text{RbOs}_2\text{O}_6$ :  $\lambda_{\text{ep}} \approx 1$ ). The estimated Sommerfeld coefficient of  $\text{KO}_{\text{Os}_2}\text{O}_6$ ,  $\gamma = 76$  to 110 mJ/(mol K<sup>2</sup>), is twice that of  $\text{RbOs}_2\text{O}_6$  [ $\gamma = 44$  mJ/(mol K<sup>2</sup>)]. Using strong-coupling corrections, we extract useful thermodynamic parameters of  $\text{KO}_{\text{Os}_2}\text{O}_6$ . Quantifying  $\lambda_{\text{ep}}$  allows us to determine the mass enhancement over the calculated band electronic density of states. A significant contribution in addition to the electron-phonon term of  $\lambda_c = 1.7$  to 4.3 is deduced. In an effort to understand the origin of the enhancement mechanism, we also investigate an unusual energetically low-lying phonon. There are three phonon modes per  $\text{RbOs}_2\text{O}_6$ , suggestive of the phonon source being the rattling motion of the alkali ion. This dynamic instability of the alkali ions causes large scattering of the charge carriers which shows up in an unusual temperature dependence of the electrical resistivity.

PACS numbers: 74.25.Bt, 74.25.Op, 74.70.-b

---

\*Electronic address: markus.bruehwiler@phys.ethz.ch

## I. INTRODUCTION

Long standing interest in the pyrochlores stems from their inherent geometrical frustration due to the metal ions forming a network of corner-sharing tetrahedra. For insulating pyrochlores, where localized magnetic moments sit on the vertices of these tetrahedra, competing interactions lead to a wealth of novel states of fundamental interest. Ground states of infinite degeneracy are a typical signature of such frustrated systems.[1, 2, 3] While for insulating systems the intimate connection between spins and the lattice topology leads to the observed frustration effects, it is an open question how charge, spin, and lattice degrees of freedom are coupled in itinerant systems and how they influence each other.

In this context, the superconductivity recently found in  $\text{KO}_{\text{S}_2}\text{O}_6$  has been of considerable interest:[4] It has been thought that a spin liquid ground state resulting from frustration in these structures might favor superconductivity through singlet pairing by a resonating valence bond.[5] At the time of its discovery,  $\text{KO}_{\text{S}_2}\text{O}_6$  was the second pyrochlore superconductor known after  $\text{Cd}_2\text{Re}_2\text{O}_7$ .[6, 7, 8] Soon after, the discovery of superconducting  $\text{Rb}_{\text{Os}_2}\text{O}_6$ [9, 10] and  $\text{Cs}_{\text{Os}_2}\text{O}_6$ [11] followed.  $\text{Cd}_2\text{Re}_2\text{O}_7$  crystallizes in the so-called  $\alpha$ -pyrochlore structure, the structure adopted by numerous insulating pyrochlores, and  $A\text{Os}_2\text{O}_6$  (where  $A = \text{Cs}, \text{Rb}$ , or  $\text{K}$ ) has the  $\beta$ -pyrochlore structure. While the  $A\text{Os}_2\text{O}_6$  compounds could be expected to be very similar in their physical properties, there is in fact quite a variation among them.

For example,  $T_c$  decreases from 9.5 K for  $\text{KO}_{\text{S}_2}\text{O}_6$  to 6.4 K for  $\text{Rb}_{\text{Os}_2}\text{O}_6$  and to 3.3 K for  $\text{Cs}_{\text{Os}_2}\text{O}_6$ . The nature of the superconducting state is still under discussion: while  $\text{Rb}_{\text{Os}_2}\text{O}_6$  appears to be a fully gapped  $s$ -wave superconductor with a critical temperature  $T_c = 6.4$  K,[12, 13, 14, 15, 16]  $\mu$ -SR measurements point towards an anisotropic or multigapped superconducting state in  $\text{KO}_{\text{S}_2}\text{O}_6$ .[17] This question has not been settled conclusively. It has been found that  $\text{KO}_{\text{S}_2}\text{O}_6$  single crystals show Bragg peaks that violate the  $\text{Fd}\bar{3}\text{m}$  symmetry and the structure has been identified as non-centrosymmetric  $\text{F}\bar{4}3\text{m}$ .[18] Furthermore, it remains to be determined to what degree the quasiparticle mass is enhanced by interactions other than those with ordinary phonons, e.g. to what extent electron-electron correlations play a role in these compounds. In order to address these questions a detailed characterization of these compounds is required.

In this paper, we present field and temperature dependent thermodynamic and transport measurements on  $\text{Rb}_{\text{Os}_2}\text{O}_6$  and  $\text{KO}_{\text{S}_2}\text{O}_6$ . The data provide evidence for a significant addi-

tional electronic mass enhancement beyond the contribution from the coupling to phonons and evidence for low-lying vibrational modes. We discuss similarities and differences between the two compounds and compile an extended list of the basic thermodynamic parameters.

## II. EXPERIMENTAL

KOs<sub>2</sub>O<sub>6</sub> single crystals have been grown by an encapsulation technique in an evacuated quartz tube. In this method, a stoichiometric amount of Os metal (Alfa Aesar, 99.9 %) and KO<sub>2</sub> (Alfa Aesar, 95 %) is thoroughly mixed in an argon filled dry box and pressed into a pellet. The pellet with a mass of 0.2 to 0.25 g is put into a quartz tube and silver oxide Ag<sub>2</sub>O (Aldrich, 99 %) is added to create an appropriate oxygen partial pressure during the synthesis. The evacuated and sealed tube is then inserted into a furnace preheated to 600 °C, kept there for 1 h, cooled to 400 °C at a rate of 5 °C/h, and then cooled to room temperature at a rate of 150 °C/h. The resulting black single crystals of size up to 0.3 mm in diameter have grown on the wall of the quartz tube and on the surface of the precursor pellet. The crystals have different shapes characteristic for the cubic structure such as octahedra or cubes. The lattice parameter refined from x-ray single crystal measurements is found to be  $a = 10.0968(8)$  Å. No signature of impurity phases like OsO<sub>2</sub> or KOsO<sub>4</sub> was found in heat capacity and magnetization measurements.

For the specific heat measurements, we have selected about five dozen of the most regularly shaped single crystals out of a single badge. The total mass of these crystals amounts to 2.12 mg (see inset to Fig. 2), which is enough to measure specific heat with a relaxation method. Special attention must be paid, however, to measure the addendum contribution as it makes up a significant fraction of the total mass. The specific heat has been measured in a physical properties measurement apparatus using an adiabatic relaxation technique (Quantum Design, PPMS). Resistivity has been measured by a standard four terminal approach also using the PPMS and the dc magnetization has been measured in a SQUID magnetometer (Quantum Design, MPMS). Measurements on RbOs<sub>2</sub>O<sub>6</sub> have been performed on a sample previously reported upon in Ref. [15]. The synthesis procedure of these polycrystalline RbOs<sub>2</sub>O<sub>6</sub> samples is described elsewhere.[4, 19]

### III. RESULTS

In order to determine the mass enhancement in the normal state and the magnitude of the electron-phonon coupling, it is necessary to measure the Sommerfeld coefficient of the superconductor by driving it into the normal state. Usually this is achieved by applying a magnetic field exceeding the upper critical field  $H_{c2}$ . Owing to a high  $H_{c2}(0\text{ K})$  of  $\text{KO}_{\text{S}_2}\text{O}_6$  which is unaccessible by our 14 T magnet, it is not possible to tune  $\text{KO}_{\text{S}_2}\text{O}_6$  into its normal state below about 6.2 K. We therefore resort to an extrapolation method to estimate the Sommerfeld coefficient: first we measure the phase boundary line  $H_{c2}(T)$  to as low a temperature and high field as possible. We then extrapolate  $H_{c2}$  to 0 K and estimate the Sommerfeld coefficient based on the measured  $C_p/T$  versus magnetic field curve at a low temperature. The details of this procedure are given in the following.

#### A. Upper critical field $H_{c2}$

We extract the upper critical field  $H_{c2}$  from  $C_p(T)$  data for  $\text{KO}_{\text{S}_2}\text{O}_6$  and from both  $C_p(T)$  and  $C_p(H)$  data for  $\text{Rb}_{\text{S}_2}\text{O}_6$ . For both methods, we use a construction of equal area to determine the critical field. The two methods result in almost identical  $H_{c2}$  as can be seen in Fig. 1. In our experience, the  $H_{c2}$  slope at  $T_c$  for both  $\text{Rb}_{\text{S}_2}\text{O}_6$  and  $\text{KO}_{\text{S}_2}\text{O}_6$  are rather stable quantities varying little from sample to sample. We therefore have a high level of confidence that the observed slope is indeed intrinsic to the material and not mainly limited by a mean free path caused by impurity scattering.

The initial slope of the critical boundary at  $T_c$  for  $\text{KO}_{\text{S}_2}\text{O}_6$  is  $-3.6\text{ T/K}$ , in agreement with the revised value in Ref. [10, 20]. The full  $H_{c2}(T)$  dependence cannot be mapped out with the 14 T magnet, so we need to extrapolate to lower temperatures and we proceed in two different ways: first, we notice that  $H_{c2}(T)$  in  $\text{Rb}_{\text{S}_2}\text{O}_6$  is rather well described by the standard WHH expression, with an initial slope of  $-1.2\text{ T/K}$  and  $\mu_0 H_{c2}(0\text{ K}) = 6\text{ T}$  (Fig. 1).[12] If we were to assume the same functional form to hold also for  $\text{KO}_{\text{S}_2}\text{O}_6$ ,  $\mu_0 H_{c2}(0\text{ K}) = 24\text{ T}$  is estimated. Considering that a typical energy of low-lying phonons in  $\text{KO}_{\text{S}_2}\text{O}_6$  is around 30 K,  $H_{c2}$  might be underestimated in this way. Alternatively, one can extrapolate linearly to  $T = 0\text{ K}$  and would estimate  $\mu_0 H_{c2}(0\text{ K}) = 35\text{ T}$ . Pursuing this second extrapolation further is motivated by our observation that the last data points in our data lie closer to

a straight line extrapolation of the lower-field data, while the WHH curve starts deviating from the data in this region. In the rest of this paper, we thus consider both extrapolations, denoting with (A) the WHH version, and with (B) the linear method. Numerical values for (B) will be enclosed in braces {}.

It is worth noting that the  $\text{RbOs}_2\text{O}_6$  data are fitted best by the WHH formula in the orbital limit ( $\lambda_{\text{SO}} = \infty$ ). This is in agreement with a large  $\lambda_{\text{SO}}$  expected for the heavy Os ion. Therefore, pair-breaking effects of the magnetic field on the spin degrees of freedom are negligible due to the randomizing effect of the spin-orbit scattering on the phase of the superconducting electrons. An upper limit of the critical field in the case where spin-orbit scattering could be ignored, is given by the Pauli-limiting field: for  $\text{KO}_2\text{O}_6$  it is  $\mu_0 H_{\text{P}} = \Delta(0 \text{ K}) / (\sqrt{2}\mu_{\text{B}})\sqrt{1 + \lambda_{\text{ep}}} \approx 37 \text{ T}$  {27 T}, while for  $\text{RbOs}_2\text{O}_6$  it is about 18 T. Here we have used the values for  $\Delta(0 \text{ K})$  and  $\lambda_{\text{ep}}$  determined from our measurements as described later and listed in Table I. For  $\text{RbOs}_2\text{O}_6$ , this field is well above the measured upper critical field, while for  $\text{KO}_2\text{O}_6$  the comparison depends on the extrapolation of  $H_{\text{c}2}$ . Support for the fact that  $H_{\text{c}2}$  is determined by the orbital motion of the electrons and not by their spin, is provided by the ratio of the slopes  $-d\mu_0 H_{\text{c}2} / dT|_{T_{\text{c}}}$  for the two materials  $\text{RbOs}_2\text{O}_6$  and  $\text{KO}_2\text{O}_6$ . The slopes are proportional to  $1/(\tau v_{\text{F}}^2)$ , where  $\tau$  is the electronic scattering time and  $v_{\text{F}}$  the Fermi velocity. For the Fermi velocities we use  $2.587 \cdot 10^7 \text{ cm/s}$  for  $\text{RbOs}_2\text{O}_6$  and  $2.671 \cdot 10^7 \text{ cm/s}$  for  $\text{KO}_2\text{O}_6$ . [21] The ratio of the Fermi velocities squared, taking into account the renormalization of the Fermi velocity and assuming the same  $\tau$  for both materials, is 2.4 {4.7}. This is indeed close to the ratio of  $-d\mu_0 H_{\text{c}2} / dT|_{T_{\text{c}}}$  for  $\text{RbOs}_2\text{O}_6$  and  $\text{KO}_2\text{O}_6$ :  $3.6/1.2 = 3$ , suggesting that the pair-breaking is caused conventionally by the effect of the magnetic field on the orbital magnetism of the electrons. The difference in magnitude of the upper critical fields is therefore in line with the different mass enhancements.

## B. Heat capacity in a magnetic field

We have measured the field dependence of  $C_{\text{p}}/T$  of  $\text{KO}_2\text{O}_6$  at 0.46 K, shown in Fig. 2. The addendum is  $\approx 10\%$  of the total heat capacity at  $\mu_0 H = 14 \text{ T}$ ,  $\approx 20\%$  at  $\mu_0 H = 7 \text{ T}$ , and  $\approx 50\%$  at  $\mu_0 H = 3 \text{ T}$ . Below  $\mu_0 H = 1.7 \text{ T}$ , the addendum makes up more than 90% of the total heat capacity, and even though both data sets are very smooth, this leads to relatively larger scatter after taking the difference of the two data sets. For this reason, data

below 1.7 T have been omitted in the graph and in the fitting procedure.

We parameterize the measured curve by  $C_p/T = a(H/\text{Oe})^b + c$ . A least squares fit down to 1.75 T using this form results in  $a = (5.86 \pm 1.3) \cdot 10^{-4} \text{ mJ}/(\text{mol K}^2)$ ,  $b = 0.9512 \pm 0.02$ , and  $c = -0.35 \pm 0.4 \text{ mJ}/(\text{mol K}^2)$ , where  $H$  is given in Oersted. An extrapolation of the  $C_p(H)$  curve at 0.46 K to the upper critical field  $H_{c2}$  of 24 T {35 T} results in a rather high Sommerfeld coefficient for  $\text{KO}_{\text{Os}_2}\text{O}_6$  of  $\gamma = 76 \text{ mJ}/(\text{mol K}^2)$  {110 mJ/(mol K<sup>2</sup>)}.

The fact that we have measured a vanishingly small  $C_p/T$  at  $H = 0 \text{ Oe}$  and  $T = 0.46 \text{ K}$  is of significance for the interpretation of the electronic and vibrational excitation spectrum. First, it indicates that the superconducting state affects the entire electronic system that gives rise to the large  $\gamma$  value [76 to 110 mJ/(mol K<sup>2</sup>)]. Secondly, the vibrational excitation spectrum (at 0.46 K) is not characterized by a glass-like spectrum ( $C_p \propto T$ ) as one might expect from a broad distribution of 2-level configurations possibly associated with the particular lattice potential experienced by the K ions.[22]

In addition to estimating the Sommerfeld coefficient, measurements of the magnetic field dependent heat capacity can be helpful to reveal nodes in the gap function. It is generally thought that a square root dependence  $C_p/T \propto H^\alpha$  with  $\alpha = 1/2$  indicates a gap with nodes, while a linear dependence  $\alpha = 1$  indicates a fully gapped state.[23] This is because the electronic excitations in the vortex state of conventional superconductors are predominantly low-energy excitations localized in the vortex core. On the other hand, the density of states for superconductors with lines of gap nodes results mostly from delocalized states outside the vortex which are located in the vicinity of the gap nodes in momentum space.

We expect that the exponent in the above fit to  $C_p$  versus  $H$  tends even closer toward 1 as  $T \rightarrow 0 \text{ K}$ , since the exponent decreases when measuring at increasingly higher temperatures (data not shown). The field-dependence of the heat capacity of  $\text{KO}_{\text{Os}_2}\text{O}_6$  thus appears to be in line with a fully gapped state. However, since the measurements do not extend up to  $H_{c2}$ , further experimental evidence is needed to settle this point conclusively.

### C. Density of states and mass enhancement

The specific heat for  $\text{KO}_{\text{Os}_2}\text{O}_6$  in various fields is shown in Fig. 3. In addition to the anomaly indicating the transition into the superconducting state, there are two additional peaks at  $T_{p,1}$  ( $\approx 6.5 \text{ K}$ ) and  $T_{p,2}$  ( $\approx 7 \text{ K}$ ). The origin of these peaks is unclear at this point.

They are likely to be associated with the dynamics of the potassium ions in this compound. While we measure two peaks for our sample, a single peak has been reported in Ref. [10, 20] at a slightly higher temperature (about 7.5 K) - the transition seems to be very sensitive to microscopic details.

From the specific heat jump at  $T_c$ ,  $\Delta C_p|_{T_c}/T_c = 204 \text{ mJ}/(\text{mol K}^2)$ , the normalized specific heat jump  $\Delta C_p|_{T_c}/(\gamma T_c) = 2.7 \{1.9\}$  is extracted. It is significantly larger than in the weak-coupling limit and corresponds to an electron-phonon coupling constant  $\lambda_{\text{ep}} = 2 \int_0^\infty \alpha^2 F(\omega)/\omega d\omega \approx 1.6 \{1.0\}$ , [24] i.e.  $\text{KO}_{\text{Os}_2}\text{O}_6$  is a superconductor in the strong-coupling regime. Here,  $\alpha^2 F(\omega)$  is the spectral density of the electron-phonon coupling function. Using the calculated band Sommerfeld coefficient  $\gamma_b = 9.8 \text{ to } 11.36 \text{ mJ}/(\text{mol K}^2)$  of  $\text{KO}_{\text{Os}_2}\text{O}_6$  from Refs. [22, 25], this result indicates a significant enhancement of the electronic specific heat of  $(1 + \lambda_{\text{ep}})(1 + \lambda_c) = [76 \text{ mJ}/(\text{mol K}^2)]/[10.6 \text{ mJ}/(\text{mol K}^2)] \approx 7.2 \{10.4\}$ , i.e. about double the enhancement found in  $\text{Sr}_2\text{RuO}_4$  of 3.8 to 4. [26, 27] This quantification of  $\lambda_{\text{ep}}$  then leaves a significant additional enhancement  $\lambda_c \approx 1.7 \{4.3\}$  ascribed to electron-electron correlations.

Figure 4 illustrates the density of states for  $\text{KO}_{\text{Os}_2}\text{O}_6$  and  $\text{RbOs}_2\text{O}_6$  and the weak-coupling  $\alpha$ -pyrochlore superconductor  $\text{Cd}_2\text{Re}_2\text{O}_7$  for comparison. The depicted band density of states for  $\text{AO}_{\text{Os}_2}\text{O}_6$  is the arithmetic mean of the two calculated values in Refs. [22, 25], and the values for  $\text{Cd}_2\text{Re}_2\text{O}_7$  are taken from Refs. [6, 28]. It increases very slightly on going from  $A=\text{K}$  to  $A=\text{Rb}$  to  $\text{Cd}_2\text{Re}_2\text{O}_7$ , but is rather similar overall. The electronic structure in the LDA as a whole is in fact very similar for all  $\text{AO}_{\text{Os}_2}\text{O}_6$ . The electron-phonon enhancement, on the other hand varies significantly:  $\lambda_{\text{ep}}$  is less than about 0.4 for  $\text{Cd}_2\text{Re}_2\text{O}_7$ , but falls in the intermediate to strong-coupling range for the osmates (1 to 1.6), indicating that there is a significant difference in the coupling functions leading to the superconducting state. The difference in the additional enhancement  $\lambda_c$  is pronounced: it increases more than twofold from  $\text{RbOs}_2\text{O}_6$  to  $\text{KO}_{\text{Os}_2}\text{O}_6$ , in the same direction as  $\lambda_{\text{ep}}$ .

To gain further insight into the mechanisms responsible for the density of states enhancement, it is helpful to consider the magnetic susceptibility (Fig. 5). Since samples of  $\text{RbOs}_2\text{O}_6$  also contain some  $\text{OsO}_2$ , the intrinsic magnetic susceptibility is calculated according to  $\chi_1 = \eta_m^{-1}\chi - (\eta_m^{-1} - 1)\chi_2$ , where  $\chi_1$  is the magnetic susceptibility of  $\text{RbOs}_2\text{O}_6$ ,  $\chi_2$  that of  $\text{OsO}_2$ , and  $\chi$  is the measured susceptibility of the mixed system (c.f. Sec. III E). The susceptibilities in this formula are given per mass. The correction due to  $\text{OsO}_2$  is very small, since the susceptibility per Os is very similar in both systems. Even after taking into account

the correction for  $\text{OsO}_2$ , the susceptibility of  $\text{RbOs}_2\text{O}_6$  still shows a slight increase at low temperatures and also a shoulder around 25 K. This is probably due to minute amounts of magnetic  $\text{RbOsO}_4$ . We note that a similar  $T$  dependence as for the susceptibility has been observed for the Knight shift in both  $\text{RbOs}_2\text{O}_6$  and  $\text{KOs}_2\text{O}_6$ .[29]

We correct for the diamagnetism of the core using  $\chi = \chi_{\text{exp}} - \chi_{\text{core}}$  with  $\chi_{\text{core}} = -12, -20, -13$ , and  $-18 \mu\text{cm}^3/\text{mol}$  for  $\text{O}^{2-}$ ,  $\text{Rb}^+$ ,  $\text{K}^+$ , and  $\text{Os}^{6+}$  ions respectively. Landau diamagnetism can be neglected, due to the enhancement of the electron mass. For the experimental susceptibility, we use the value at 150 K, resulting in a susceptibility for  $\text{KOs}_2\text{O}_6$  of  $\chi^{\text{emu}} \approx 3.7 \cdot 10^{-4} \text{ cm}^3/\text{mol}$ . The Sommerfeld-Wilson ratio evaluates to  $R_W = 0.93 \text{ G}^2 \text{ cm}^3/\text{erg} \{0.65 \text{ G}^2 \text{ cm}^3/\text{erg}\}$  where we have used the renormalized Sommerfeld coefficient  $\gamma/(1 + \lambda_{\text{ep}})$  since the Pauli magnetic susceptibility is not affected by electron-phonon interactions. For  $\text{RbOs}_2\text{O}_6$  follows  $\chi^{\text{emu}} \approx 5.3 \cdot 10^{-4} \text{ cm}^3/\text{mol}$  and  $R_W = 1.75 \text{ G}^2 \text{ cm}^3/\text{erg}$ . In view of a calculated Stoner enhancement of the magnetic susceptibility of roughly 2 for all  $AOs_2O_6$  (Refs. [22, 25]), the Wilson ratio for  $\text{RbOs}_2\text{O}_6$  closely matches the expected result. On the other hand,  $R_W$  for  $\text{KOs}_2\text{O}_6$  is clearly smaller than what would be expected. In this simple estimate, we have neglected possible orbital van Vleck terms that may also contribute to the paramagnetic susceptibility.

#### D. Superconducting Properties

It is instructive to calculate the various thermodynamic parameters for  $\text{KOs}_2\text{O}_6$  and  $\text{RbOs}_2\text{O}_6$ . We get a strong-coupling parameter  $x := k_B T_c / (\hbar \omega_{\text{ln}}) = 0.13 \{0.06\}$  by applying the approximate semiphenomenological form of the strong-coupling correction to the weak coupling BCS ratio which holds for many superconductors  $\Delta C_p|_{T_c} / (\gamma T_c) = 1.43 [1 - 53x^2 \ln(3x)]$ .[30] Here  $\hbar \omega_{\text{ln}}$  is the Allen-Dynes expression for the average phonon energy. With this strong-coupling parameter we further get a normalized energy gap of  $2\Delta(0 \text{ K}) / (k_B T_c) = 3.53 [1 - 12.5x^2 \ln(2x)] = 4.57 \{3.83\}$ . Since we know from  $\text{RbOs}_2\text{O}_6$  that another strong-coupling correction,  $1/(8\pi) \cdot \gamma T_c^2 / (-\Delta F) = 0.168 [1 + 12.2x^2 \ln(3x)]$ , holds quite well,[15] it is reasonable to assume that it also holds for  $\text{KOs}_2\text{O}_6$ . Using the experimental  $T_c$ ,  $\gamma$ , and the strong-coupling parameter from above, we can estimate the condensation energy of  $\text{KOs}_2\text{O}_6$ :  $-\Delta F = 2050 \text{ mJ/mol} \{2533 \text{ mJ/mol}\}$ , corresponding to a thermodynamic critical field of  $H_c = 2579 \text{ Oe} \{2867 \text{ Oe}\}$ . In this conversion we have used the

TABLE I: Thermodynamic parameters of the superconductors  $\text{KO}_{\text{S}_2}\text{O}_6$  and  $\text{Rb}_{\text{S}_2}\text{O}_6$ .

Parameter	$\text{KO}_{\text{S}_2}\text{O}_6$	$\text{Rb}_{\text{S}_2}\text{O}_6$
$T_c$	9.5 K	6.4 K
$\xi(0\text{ K})$	37 Å {31 Å}	74 Å
$\lambda_{\text{eff}}(0\text{ K})$	243 nm {265 nm}	252 nm
$\kappa(T_c), \kappa(0\text{ K})$	45, 66 {45, 86}	23, 34
$\gamma$	76 {110} mJ/(mol <sub>f.u.</sub> K <sup>2</sup> )	44 mJ/(mol <sub>f.u.</sub> K <sup>2</sup> )
$\Delta C_p _{T_c}/(\gamma T_c)$	2.7 {1.9}	1.9
$\lambda_{\text{ep}}$	1.6 {1.0}	1.0
$\lambda_c$	1.7 {4.3}	1.0
$b$	0.95 K <sup>-1</sup> {0.77 K <sup>-1</sup> }	1.12 K <sup>-1</sup>
$b/T_c$	0.099 K <sup>-2</sup> {0.080 K <sup>-2</sup> }	0.175 K <sup>-2</sup>
$bT_c$	9.021 {7.299}	7.168
$-\Delta F(0\text{ K})$	2050 {2533} mJ/mol <sub>f.u.</sub>	483 mJ/mol <sub>f.u.</sub>
$H_c(0\text{ K})$	2579 Oe {2867 Oe}	1249 Oe
$H_{c1}(0\text{ K})$	116 Oe {105 Oe}	92 Oe
$\mu_0 H_{c2}(0\text{ K})$	24 T {35 T}	6 T
$-\text{d}H_c/\text{d}T _{T_c}$	575 Oe/K	369 Oe/K
$-\text{d}\mu_0 H_{c2}/\text{d}T _{T_c}$	3.6 T/K	1.2 T/K
$Q \equiv -\frac{2T_c}{H_c(0)} \frac{\text{d}H_c}{\text{d}T} _{T_c}$	4.25 {3.82}	3.79
$k_B T_c/(\hbar\omega_{\text{ln}})$	0.13 {0.06}	0.06
$2\Delta(0\text{ K})/(k_B T_c)$	4.57 {3.83}	3.87
$1/(8\pi) \cdot \gamma T_c^2/(-\Delta F)$	0.13 {0.16}	0.15

calculated mass density of  $\text{KO}_{\text{S}_2}\text{O}_6$  using the lattice constant from x-ray,  $\rho = 6.653 \text{ g/cm}^3$ . The ratio  $1/(8\pi) \cdot (\gamma T_c^2)/(-\Delta F)$  itself evaluates to 0.135 {0.157}.

Once the condensation energy is known, various thermodynamic quantities can be evaluated: for  $bT_c \equiv (T\Delta C_p)|_{T_c}/(-\Delta F)$  we get 9.02 {7.30}, giving a normalized critical field slope  $Q = 4.25$  {3.82}. The critical field slope itself evaluates to  $-\text{d}H_c/\text{d}T|_{T_c} = 575 \text{ Oe/K}$ . The slope of the upper critical field is about 3 times steeper than the one from  $\text{Rb}_{\text{S}_2}\text{O}_6$ : with  $-\text{d}\mu_0 H_{c2}/\text{d}T|_{T_c} = 3.6 \text{ T/K}$  (Fig. 1) we get a Ginzburg-Landau parameter at the critical

temperature of  $\kappa(T_c) = 45$ . At  $T \rightarrow 0$  K, we estimate  $\kappa(0$  K) =  $1/\sqrt{2} \cdot H_{c2}/H_c = 66$  {86} and thus a penetration depth of 243 nm {265 nm}, which compares well with results from  $\mu$ -SR experiments (270 nm).[17] The Ginzburg-Landau coherence length amounts to  $\xi = 37$  Å {31 Å} and the lower critical field  $H_{c1} = \ln \kappa/(\sqrt{2}\kappa)H_c = 116$  Oe {105 Oe}. This lower critical field is in agreement with magnetization measurements (not shown). The Ginzburg-Landau coherence length is about half that of RbOs<sub>2</sub>O<sub>6</sub>. The parameters are listed in Table I, where they are compared to the values of RbOs<sub>2</sub>O<sub>6</sub> taken from Ref. [15] for convenience.

$H_{c2}$  for KOs<sub>2</sub>O<sub>6</sub> is beyond the 14 T accessible in our current setup, so that the samples cannot be tuned to the normal state below about 6.2 K. There is thus no reference measurement for the heat capacity in the normal state and the superconducting electronic specific heat  $C_{es}$  cannot be determined by a simple subtraction of a normal state and a superconducting state measurement. This renders determining additional contributions to the heat capacity other than the usual phononic and electronic terms difficult.

### E. Unusual low-energy atomic vibrations

The specific heat of RbOs<sub>2</sub>O<sub>6</sub> is analysed using the condensation energy analysis (CEA) developed in Ref. [15]. This is necessary because it is not yet possible to synthesize a fully phase pure RbOs<sub>2</sub>O<sub>6</sub> sample. OsO<sub>2</sub> has been identified by x-ray diffraction analysis as a secondary phase. This shortcoming is compensated by the fact that by using the CEA it is possible to extract the intrinsic properties of superconducting RbOs<sub>2</sub>O<sub>6</sub> even if the samples contain some unreacted OsO<sub>2</sub> starting material.

The full temperature dependence of the intrinsic heat capacity of RbOs<sub>2</sub>O<sub>6</sub> is therefore obtained by subtracting the appropriate amount of the OsO<sub>2</sub> heat capacity contribution according to  $C_1 = \eta_m^{-1}C - (\eta_m^{-1} - 1)C_2$ . Here,  $C_1$  is the heat capacity of RbOs<sub>2</sub>O<sub>6</sub>,  $C_2$  of OsO<sub>2</sub>, and  $C$  is the measured heat capacity of the mixed system, all in energy per temperature per mass. To this end we have measured a sample of the starting material OsO<sub>2</sub>. Its heat capacity is shown in Fig. 6 ( $C_2$ ) together with the heat capacity of a RbOs<sub>2</sub>O<sub>6</sub> sample ( $C$ ) with a superconducting mass fraction of  $\eta_m = 74.9\%$ . Hence, the difference between the mixed system heat capacity  $C$  and 25.1 % of  $C_2$  (shaded region) is 74.9 % of the intrinsic heat capacity of RbOs<sub>2</sub>O<sub>6</sub>  $C_1$ . The Sommerfeld coefficients used in the plot are  $\gamma = 27.5 \mu\text{J}/(\text{g K}^2)$  for OsO<sub>2</sub> and  $\gamma = 70.3 \mu\text{J}/(\text{g K}^2)$  for the RbOs<sub>2</sub>O<sub>6</sub> sample.

The resulting specific heat of  $\text{RbOs}_2\text{O}_6$  ( $C_1$ ) on a logarithmic temperature scale is shown in Fig. 7. In such a plot, an Einstein contribution to the heat capacity appears as a bell-shaped feature with a peak at  $T = T_E/4.93$ .[31] The data clearly indicate such a contribution with an Einstein temperature of 60 K and a density of  $0.33 \cdot 9$  modes/f.u.. Assuming this phonon involves the displacement of the Rb atoms, this means an effective number of 3 modes per Rb ion. Three modes are compatible with a 3-dimensional potential for the Rb ions to move in as is expected from the tetrahedral symmetry of the Rb site.

As the  $\text{KO}_2\text{O}_6$  samples are high-quality single crystals, the  $\text{KO}_2\text{O}_6$  data can be analyzed as measured. We have observed a vanishingly small residual Sommerfeld coefficient ( $C_p/T \rightarrow -0.35 \pm 0.4 \text{ mJ}/(\text{mol K}^2)$  as  $H \rightarrow 0 \text{ Oe}$  at 0.46 K) as expected from a single phase sample and indicative of a fully gapped electronic excitation spectrum. The temperature dependent lattice heat capacity data is shown in Fig. 8. In the normal state above 6.2 K,  $\gamma T$  was used for the electronic heat capacity  $C_{\text{el}}$ . The low temperature data from 2 to 3.8 K were obtained using the electronic heat capacity of an isotropic superconductor  $C_{\text{el}} = C_{\text{es}} = 8.5 \gamma T_c \exp(-1.44 \cdot 2\Delta(0 \text{ K})/3.53 \cdot T_c/T)$ . The data does not fit as nicely to a combined Debye-Einstein model as does the data for  $\text{RbOs}_2\text{O}_6$ . This might be due to the alkali-ion potential being very anharmonic, leading to a vibrational spectrum that is not simply modeled by an Einstein mode. Nevertheless, we show a best fit of an Einstein contribution to the data in the figure, resulting in  $n = 0.15 \cdot 9$  modes/f.u. and  $T_E = 31 \text{ K}$ . For the Debye contribution which is expected to result mainly from the rigid Os-O network we have reused the Debye temperature from  $\text{RbOs}_2\text{O}_6$ . The question about the low-energy lattice dynamics appears to be central to the physics of  $\text{KO}_2\text{O}_6$ . The calculated anharmonic potential for the K ion results in a set of discrete vibrational energies, leading to a distinct  $T$  dependence of the specific heat.[32] The data deviates markedly from this model calculation at low temperature (Fig. 8). Possibly, this indicates a freezing of the dynamic motion of the alkali ion.

## F. Resistivity

As has been noted before,[4] the resistivity of  $\text{KO}_2\text{O}_6$  shows a peculiar downward curvature, which extends to the lowest measured temperatures. This downward curvature also exists in the other  $AO_2\text{O}_6$  compounds, though at different temperatures: the curve looks

like an additional hump superimposed on a more smooth background, the hump having its peak at a temperature shifting systematically to higher temperatures on going from  $A=K$  to  $A=Cs$ . We analyze this behavior by taking the derivative of the resistivity with respect to temperature and then locating the maximum of the resulting curve. Owing to varying effective geometric factors due to grain sizes, the absolute values of the resistivities among samples vary significantly. In Fig. 9 we therefore show the normalized derivative of the resistivity where we have set the peak value to unity.

For illustrative purposes, we compare these results with a model calculation for the resistivity caused by an Einstein phonon:[33]

$$\rho_{ph} = \frac{2\pi m^* \alpha^2 F_E}{ne^2} \frac{\coth(T_E/(2T))}{1 + 2/3 \sinh^2(T_E/(2T))}, \quad (1)$$

where  $m^*$  is the averaged band mass,  $\alpha^2 F_E$  is an Einstein spectral function,  $n$  is the number of conduction electrons per unit volume,  $e$  is the elementary charge, and  $k_B T_E$  is the energy of the Einstein mode. The inset of Fig. 9 shows the derivative of the model resistivity for a peak at 50 K. It describes the data well at low temperatures, but deviates at higher temperatures, where the model predicts a resistivity linear in  $T$ .

The resulting temperatures  $T_{peak}$  at which  $d\rho/dT$  peaks are plotted in Fig. 10 versus  $T_{Einstein}$ , the energy of the Einstein phonon mode extracted from the heat capacity measurement.  $T_{Einstein} \approx 70$  K for  $CsOs_2O_6$  is taken from Ref. [10, 34]. It can be shown that the derivative of the model resistivity  $d\rho_{ph}/dT$  shows a maximum at  $T_{peak} = T_E/a$ , where  $a \approx 2.243$ .[43] For illustrative purposes, this line is shown along the experimental results from  $AOs_2O_6$  in Fig. 10. As one might expect, this simple Einstein phonon model is not sufficient to describe the entire  $\rho(T)$  curves, because scattering at other phonons is not included. If a second phonon is considered and the resulting resistivity is assumed to be simply the sum of the two single-phonon results according to Matthiessen's rule, then the location of the peak moves more toward the measured points: in an analysis of the specific heat data, Hiroi *et al.*[10, 34] have explained their data using a second phonon at around 140 K for  $RbOs_2O_6$  and around 175 K for  $CsOs_2O_6$ . Including a phonon at these temperatures moves the peak location up in temperature to 51 K for  $RbOs_2O_6$  and 64 K for  $CsOs_2O_6$ , shown by blue stars and arrows in Fig. 10. The deviation of the  $CsOs_2O_6$   $T_{peak}$  towards even higher temperatures may be due to the fact that at these temperatures a significant contribution to the phonon spectrum already stems from the Debye-phonons neglected up to now in the

transport model. The overall trend, however, is well represented by such an analysis and it points to the significant scattering by the  $A$  atoms.

#### IV. DISCUSSION

The systematic variation of the position of the maximum slope in the resistivity indicates a close connection between the dynamics of the alkali ion  $A$  and the electronic transport properties.  $\text{KO}_{\text{s}}\text{O}_6$  is somewhat different from the other two compounds, because its peak temperature is lower than expected from the simple Einstein phonon model (Fig. 10). This might be a result of the strong anharmonicity of the cage potential. It is known that the alkali ions move in a strongly anharmonic potential and couple to the conduction electrons owing to their large excursion from equilibrium, and previous results have been interpreted in this scenario.[10, 34]. This results in the electron-phonon coupling parameter  $\lambda_{\text{ep}}$  to increase, driving  $\text{KO}_{\text{s}}\text{O}_6$  more towards the strong-coupling regime. Electron scattering from the alkali mode as the reason for the downward curvature of the resistivity has been suggested before by Kuneš *et al.*, (Ref. [22]). While the scattering at phonons seems to be the most plausible mechanism at this point, other scenarios for the peculiar behavior of the resistivity are also conceivable: Fermi surface nesting has been found in  $\text{KO}_{\text{s}}\text{O}_6$  and has been proposed as the driving force for strong spin fluctuations.[35] It remains to be worked out in detail to what degree such fluctuations or even more exotic excitations could account for the measured resistivity. We note, however, that the static susceptibility of  $\text{KO}_{\text{s}}\text{O}_6$  is not significantly enhanced; rather it is smaller than expected based on the band density of states.

In the following we try to identify the various contributions to the measured mass enhancement reflected in the Sommerfeld coefficient  $\gamma$ . It is known that Coulomb and electron-phonon effects in a metal can be combined in a multiplicative fashion.[36] An interpretation of the additional enhancement in terms of Coulomb correlations would therefore mean a parametrization according to  $1 + \lambda = (1 + \lambda_{\text{ep}})(1 + \lambda_c)$ . In this interpretation the over-all bandwidth is reduced by a factor of  $1 + \lambda_c$  due to electron-electron interactions. The resulting Coulomb enhancement parameter  $\lambda_c$  for  $\text{RbOs}_2\text{O}_6$  is  $\approx 1.0$  and for  $\text{KO}_{\text{s}}\text{O}_6$  it is  $\approx 1.7$  {4.3}, from which we estimate the interaction strength: assuming a conduction electron density of  $n = 2$  electrons per Os, we can make a crude estimate of the Coulomb interaction potential:

$V_c = n\lambda_c/N(0) \approx 2 \text{ eV}$  for  $\text{RbOs}_2\text{O}_6$  and  $3 \text{ eV}$   $\{9 \text{ eV}\}$  for  $\text{KO}_2\text{O}_6$ . Here,  $N(0) = g(E_F)/2$  is the density of states at the Fermi level for one spin direction. Both of these values indicate a large electron correlation.

It is instructive to compare the  $A\text{Os}_2\text{O}_6$  series with a Ru based  $\alpha$ -pyrochlore series, where variations of the Ru-O-Ru angle results in a drastic change of the density of states. The compound  $\text{Y}_{2-x}\text{Bi}_x\text{Ru}_2\text{O}_7$  is a Mott insulator for small  $x$  and a normal paramagnetic metal for  $x \approx 2$ . The band Sommerfeld coefficient of  $\text{Bi}_2\text{Ru}_2\text{O}_7$  is calculated to be  $8.0 \text{ mJ}/(\text{mol K}^2)$ [37], resulting in a very small mass enhancement ( $\lambda \approx 0.23$ ). The correlations increase upon Y substitution resulting in an increase of the Sommerfeld coefficient from about  $10 \text{ mJ}/(\text{mol K}^2)$  at  $x \approx 2$  to almost  $90 \text{ mJ}/(\text{mol K}^2)$  at  $x \approx 0.9$ .[38] The enhancement at  $x = 0.9$  is thus substantial:  $\lambda \approx 10$ . Below this critical value correlations become so strong that a gap opens in the density of states and the Sommerfeld coefficient decreases rapidly and vanishes in the Mott insulating state. Using the same arguments as above for  $A\text{Os}_2\text{O}_6$ , the interaction potential  $V_c$  in  $\text{Y}_{1.1}\text{Bi}_{0.9}\text{Ru}_2\text{O}_7$  is of the order of  $10 \text{ eV}$ , certainly large enough to cause a gap for a bandwidth of typically  $3 \text{ eV}$ . At the same time the Ru-O-Ru angle is reduced from about  $139^\circ$  for  $\text{Bi}_2\text{Ru}_2\text{O}_7$  to  $129^\circ$  for  $\text{Y}_2\text{Ru}_2\text{O}_7$ .[39] This strongly indicates that a decreasing  $B$ -O- $B$  angle causes the band to narrow and the correlations among conduction electrons to increase.  $A\text{Os}_2\text{O}_6$  shows the same tendency: the Os-O-Os angle in  $\text{RbOs}_2\text{O}_6$  is  $139.4^\circ$  [ $\gamma = 44 \text{ mJ}/(\text{mol K}^2)$ ], while that for  $\text{KO}_2\text{O}_6$  is  $137.9^\circ$  [ $\gamma = 76$  to  $110 \text{ mJ}/(\text{mol K}^2)$ ]. We thus interpret the mass of  $A\text{Os}_2\text{O}_6$  to be increasingly enhanced by electron correlations going from  $A=\text{Cs}$  to  $A=\text{K}$ . Possibly the correlations are especially strong in some subband, leading to a CDW like or orbitally ordered state at around  $7 \text{ K}$  ( $T_{p,1}$  and  $T_{p,2}$  in Fig. 3).

This is consistent with another series of pyrochlores: according to Solovyev (Ref. [40]), a decreasing Mo-O-Mo angle in  $R_2\text{Mo}_2\text{O}_7$  reduces the interaction between  $\text{Mo}(\text{t}_{2g})$  orbitals which is mediated by  $\text{O}(2\text{p})$  states, causing diminishing overlap and thus enhanced mass. Although this author finds the lattice parameter to be the relevant parameter determining the physics of the compound, the physical properties of various pyrochlores appear to be more appropriately parameterized by the Mo-O-Mo angle.

An effective Hubbard  $U$  of  $2 \text{ eV}$  is in line with other transition metals. According to [28], this is not enough to classify  $\text{Cd}_2\text{Os}_2\text{O}_7$  as a strongly correlated system. In Ref. [40], however, a  $U$  of  $1.5$  to  $2.5 \text{ eV}$  explains the Mott-insulating properties of  $R_2\text{Mo}_2\text{O}_7$  very well. This might be a somewhat weak argument, because  $\text{Cd}_2\text{Os}_2\text{O}_7$  is a 5d material while

$R_2\text{Mo}_2\text{O}_7$  is 4d, which are usually more strongly correlated. On the other hand, the LDA bandwidth of  $A\text{Os}_2\text{O}_6$  is in the region of  $W \approx 3\text{ eV}$ [22, 35] and the interaction potential  $V_c$  is therefore comparable to  $W$  and thus the Mott-Hubbard localization concept is applicable. The anomalous pressure dependence of the superconducting transition temperature is in line with these findings:[41] Hydrostatic pressure reduces the correlations working against superconductivity, thus initially increasing the critical temperature. For this reason it would be of interest to see if  $\text{NaOs}_2\text{O}_6$  shows metallic or insulating behavior.

It is enlightening to compare the electronic structure of  $A\text{Os}_2\text{O}_6$  to the one of  $\text{OsO}_2$ , since, in a (limited) way,  $\text{OsO}_2$  can be regarded as  $A\text{Os}_2\text{O}_6$  without the  $A$ . It has a rutile structure with the  $\text{OsO}_6$  octahedra sharing edges in the  $c$  direction and corners in the plane perpendicular to  $c$ .[42] While the Os-Os distance to the neighboring octahedron with the shared edge and the length of the shared edge itself are shorter than the Os-Os and O-O distances in  $A\text{Os}_2\text{O}_6$ , all other Os-O, O-O, and Os-Os distances in  $\text{OsO}_2$  are slightly longer than the ones in  $A\text{Os}_2\text{O}_6$ . The Os-O-Os angles in  $\text{OsO}_2$  are  $105.0^\circ$  along the  $c$  axis and  $127.5^\circ$  perpendicular to it. Pyrochlores with a  $B$ -O- $B$  angle around  $127^\circ$  usually are in an insulating state. Directional resistivity measurements on  $\text{OsO}_2$  could thus be quite insightful in this respect.

The density of states at the Fermi level for  $\text{OsO}_2$  of about 13 to 15 states/(u.c. Ry spin) from the band structure calculation in Ref. [42] results in a Sommerfeld coefficient  $\gamma_b \approx 2.4\text{ mJ}/(\text{mol K}^2)$ . We measure a  $\gamma$  of about  $6.1\text{ mJ}/(\text{mol K}^2)$ , resulting in a specific heat enhancement of about  $1 + \lambda = 6.1/2.4 \approx 2.5$ . Assuming a small electron phonon coupling in  $\text{OsO}_2$  of  $\lambda_{\text{ep}} \approx 0.2$  and an enhancement of the form  $\gamma/\gamma_b = (1 + \lambda_{\text{ep}})(1 + \lambda_c)$ , this results in an enhancement due to correlations of  $\lambda_c \approx 1.1$ . This is quite a large enhancement parameter similar to the one of  $A\text{Os}_2\text{O}_6$ , providing further evidence that the Coulomb correlations are inherent to the Os-O system.

Recent calculations have shown that the electronic structure does not change significantly on changing the alkali metal ion  $A$ .[25] Therefore, all these considerations point to the need to consider interactions that are not captured in the electronic structure calculations. In light of the significant electron-phonon interaction, and even stronger effects due to electron correlations, it will be of interest to further focus on the possible role played by the 3D-triangular geometry of the Os-O network. In view of the strong electron correlations, the frustrated geometry might be of importance in these materials.

We take the non-superconducting state of  $Y_{2-x}Bi_xRu_2O_7$  to be a clear indication that the additional enhancement mechanism is to be regarded separately from the pairing mechanism. Both  $AOs_2O_6$  and  $Y_{2-x}Bi_xRu_2O_7$  show significant enhancement due to correlations, but only  $AOs_2O_6$  is superconducting. The question thus remains why  $AOs_2O_6$  is superconducting and  $Y_{2-x}Bi_xRu_2O_7$  is not. The answer may lie in the electron-phonon coupling, which is unusually large in  $AOs_2O_6$ . We expect this to be due the  $\beta$ -pyrochlore instead of the  $\alpha$ -pyrochlore structure, which leaves the 16d site empty and the 8b site occupied by  $A$  instead of an oxygen atom. This should significantly modify the phonon spectrum, resulting in a large  $\lambda_{ep}$ .

## V. CONCLUSION

Our data from high quality single crystalline  $KOs_2O_6$  show that  $KOs_2O_6$  is a particularly interesting transition metal oxide: it is an intermediate to strong coupling type-II superconductor with a coupling parameter  $\lambda_{ep} \approx 1$  to 1.6.  $KOs_2O_6$  has a high Sommerfeld coefficient for a pyrochlore of 76 to 110 mJ/(mol K<sup>2</sup>). We estimate a Ginzburg-Landau coherence length  $\xi \approx 31$  to 37 Å, about half the one in  $RbOs_2O_6$  due to the renormalization of the Fermi velocity  $v_F$ . We estimate the condensation energy  $-\Delta F = 2.0$  to 2.5 J/mol. The effective mass, even after the measured strong electron-phonon renormalization is taken into account, is threefold enhanced over the LDA band mass. We interpret this as due to Coulomb correlations. The renormalization affects those electrons that are paired to form the superconducting condensate. While for  $RbOs_2O_6$  the additional heat capacity can be well characterized by an Einstein model, the contribution for  $KOs_2O_6$  is somewhat more unusual, possibly due to strong anharmonicity. We associate this special phonon with a rattling motion of the alkali ions, resulting in three modes per Rb for  $RbOs_2O_6$ . In  $KOs_2O_6$ , the absence of lattice heat capacity at low temperatures may indicate the freezing of this motion. The dynamics of the alkali ions causes large scattering of the charge carriers which shows up in an unusual temperature dependence of the electrical resistivity which varies systematically with the alkali ion.

## VI. ACKNOWLEDGMENT

We thank J. Kuneš and W. E. Pickett for helpful discussions on the calculation of the lattice vibrational spectrum and R. Saniz for providing revised values for the Fermi velocities. This study was partly supported by the Swiss National Science Foundation.

## References

---

- [1] R. Moessner, Canadian Journal of Physics **79**, 1283 (2001).
- [2] J. E. Greedan, Journal of Materials Chemistry **11**, 37 (2001).
- [3] A. P. Ramirez, Annu. Rev. Mater. Sci. **24**, 453 (1994).
- [4] S. Yonezawa, Y. Muraoka, Y. Matsushita, and Z. Hiroi, J. Phys.: Condens. Matter **16**, L9 (2004).
- [5] P. W. Anderson, Mat. Res. Bull. **8**, 153 (1973).
- [6] M. Hanawa, Y. Muraoka, T. Tayama, T. Sakakibara, J. Yamaura, and Z. Hiroi, Phys. Rev. Lett. **87**, 187001 (2001).
- [7] H. Sakai, K. Yoshimura, H. Ohno, H. Kato, S. Kambe, R. E. Walstedt, T. D. Matsuda, Y. Haga, and Y. Onuki, J. Phys.: Condens. Matter **13**, L785 (2001).
- [8] R. Jin, J. He, S. McCall, C. S. Alexander, F. Drymiotis, and D. Mandrus, Phys. Rev. B **64**, 180503 (2001).
- [9] S. Yonezawa, Y. Muraoka, Y. Matsushita, and Z. Hiroi, J. Phys. Soc. Jpn. **73**, 819 (2004).
- [10] Z. Hiroi, S. Yonezawa, J.-I. Yamaura, T. Muramatsu, Y. Matsushita, and Y. Muraoka, J. Phys. Soc. Jpn. **74**, 3400 (2005).
- [11] S. Yonezawa, Y. Muraoka, and Z. Hiroi, J. Phys. Soc. Jpn. **73**, 1655 (2004).
- [12] M. Brühwiler, S. M. Kazakov, N. D. Zhigadlo, J. Karpinski, and B. Batlogg, Phys. Rev. B **70**, 020503(R) (2004).
- [13] R. Khasanov, D. G. Eshchenko, J. Karpinski, S. M. Kazakov, N. D. Zhigadlo, R. Brütsch, D. Gavillet, D. Di Castro, A. Shengelaya, F. La Mattina, et al., Phys. Rev. Lett. **93**, 157004 (2004).

- [14] K. Magishi, J. L. Gavilano, B. Pedrini, J. Hinderer, M. Weller, H. R. Ott, S. M. Kazakov, and J. Karpinski, Physical Review B (Condensed Matter and Materials Physics) **71**, 024524 (pages 5) (2005), URL <http://link.aps.org/abstract/PRB/v71/e024524>.
- [15] M. Brühwiler, S. M. Kazakov, J. Karpinski, and B. Batlogg, Physical Review B **71**, 214517 (2005).
- [16] S. Manalo, H. Michor, G. Hilscher, M. Brühwiler, and B. Batlogg, to be published.
- [17] A. Koda, W. Higemoto, K. Ohishi, S. R. Saha, R. Kadono, S. Yonezawa, Y. Muraoka, and Z. Hiroi, J. Phys. Soc. Jpn. **74**, 1678 (2005).
- [18] G. Schuck, S. M. Kazakov, K. Rogacki, N. D. Zhigadlo, and J. Karpinski, cond-mat/0601465.
- [19] S. M. Kazakov, N. D. Zhigadlo, M. Brühwiler, B. Batlogg, and J. Karpinski, Supercond. Sci. Technol. **17**, 1169 (2004).
- [20] Z. Hiroi, S. Yonezawa, J.-I. Yamaura, T. Muramatsu, and Y. Muraoka, J. Phys. Soc. Jpn. **74**, 1682 (2005).
- [21] R. Saniz, private communication.
- [22] J. Kunes, T. Jeong, and W. E. Pickett, Physical Review B (Condensed Matter and Materials Physics) **70**, 174510 (pages 6) (2004), URL <http://link.aps.org/abstract/PRB/v70/e174510>.
- [23] G. E. Volovik, JETP Lett. **58**, 469 (1993).
- [24] F. Marsiglio, J. M. Coombes, and J. P. Carbotte, Phys. Rev. B **35**, 3219 (1987).
- [25] R. Saniz and A. J. Freeman, Physical Review B (Condensed Matter and Materials Physics) **72**, 024522 (pages 7) (2005), URL <http://link.aps.org/abstract/PRB/v72/e024522>.
- [26] D. J. Singh, Physical Review B (Condensed Matter and Materials Physics) **52**, 1358 (1995), URL <http://link.aps.org/abstract/PRB/v52/p1358>.
- [27] T. Oguchi, Physical Review B (Condensed Matter and Materials Physics) **51**, 1385 (1995), URL <http://link.aps.org/abstract/PRB/v51/p1385>.
- [28] D. J. Singh, P. Blaha, K. Schwarz, and J. O. Sofo, Phys. Rev. B **65**, 155109 (2002).
- [29] K. Arai, J. Kikuchi, K. Kodama, M. Takigawa, S. Yonezawa, Y. Muraoka, and Z. Hiroi, cond-mat/0411460.
- [30] F. Marsiglio and J. P. Carbotte, Phys. Rev. B **33**, 6141 (1986).
- [31] R. G. Chambers, Proceedings of the Physical Society **78**, 941 (1961), URL <http://stacks.iop.org/0370-1328/78/941>.

- [32] J. Kunes and W. E. Pickett, to be published in *Physica B*.
- [33] H.-L. Engquist, *Physical Review B (Condensed Matter and Materials Physics)* **21**, 2067 (1980), URL <http://link.aps.org/abstract/PRB/v21/p2067>.
- [34] Z. Hiroi, S. Yonezawa, T. Muramatsu, J.-I. Yamaura, and Y. Muraoka, *J. Phys. Soc. Jpn.* **74**, 1255 (2005).
- [35] R. Saniz, J. E. Medvedeva, L.-H. Ye, T. Shishidou, and A. J. Freeman, *Phys. Rev. B* **70**, 100505(R) (2004).
- [36] R. E. Prange and A. Sachs, *Physical Review* **158**, 672 (1967), URL <http://link.aps.org/abstract/PR/v158/p672>.
- [37] F. Ishii and T. Oguchi, *J. Phys. Soc. Jpn.* **69**, 526 (2000).
- [38] S. Yoshii and M. Sato, *J. Phys. Soc. Jpn.* **68**, 3034 (1999).
- [39] R. Kanno, Y. Takeda, T. Yamamoto, Y. Kawamoto, and O. Yamamoto, *Journal of Solid State Chemistry* **102**, 106 (1993).
- [40] I. V. Solovyev, *Physical Review B (Condensed Matter and Materials Physics)* **67**, 174406 (pages 15) (2003), URL <http://link.aps.org/abstract/PRB/v67/e174406>.
- [41] T. Muramatsu, N. Takeshita, C. Terakura, H. Takagi, Y. Tokura, S. Yonezawa, Y. Muraoka, and Z. Hiroi, *Physical Review Letters* **95**, 167004 (pages 4) (2005), URL <http://link.aps.org/abstract/PRL/v95/e167004>.
- [42] L. F. Mattheiss, *Physical Review B* **13**, 2433 (1976).
- [43]  $a$  is the nonzero solution of  $2 \sinh(a/2) + 5a \cosh(a/2) - 18a \cosh^3(a/2) + 16 \sinh(a/2) \cosh^6(a/2) - 8a \cosh^7(a/2) + 12a \cosh^5(a/2) = 0$ .

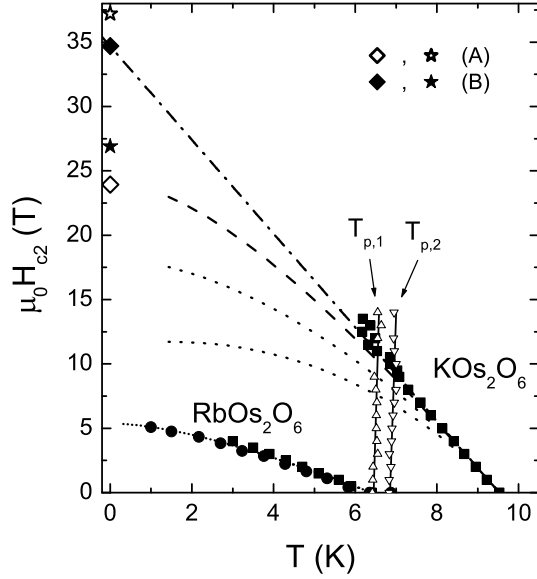


FIG. 1: The upper critical field  $H_{c2}(T)$  of  $\text{KO}_{\text{s}2}\text{O}_6$  and  $\text{Rb}_{\text{s}2}\text{O}_6$ . The squares (■) are data points extracted from  $C_p/T$  versus  $T$  data, while the circles (●) are extracted from  $C_p/T$  versus  $H$  data. For  $\text{KO}_{\text{s}2}\text{O}_6$ , two methods to extrapolate to 0 K are used: (A) The dashed line is from the WHH formula in the orbital limit ( $\lambda_{\text{SO}} = \infty$ ), providing a good description of the data up to about 9 T, while a description with smaller spin-orbit scattering strength (dotted lines) deviates markedly. (B) The dash-dotted line is a linear fit to the data. The stars mark the Pauli-limiting field  $\mu_0 H_P$  for  $\text{KO}_{\text{s}2}\text{O}_6$ .  $T_{p,1}$  and  $T_{p,2}$  mark two additional peaks observed in the specific heat (Fig. 3) that might be associated with K ordering.

FIG. 2: (Color online) Heat capacity versus magnetic field of  $\text{KO}_{\text{s}2}\text{O}_6$  at 0.46 K. An extrapolation to the upper critical field  $H_{c2} \approx 24$  T {35 T} results in a Sommerfeld coefficient  $\gamma = 76 \text{ mJ}/(\text{mol K}^2)$  { $\gamma = 110 \text{ mJ}/(\text{mol K}^2)$ }. The inset shows the measured crystals.

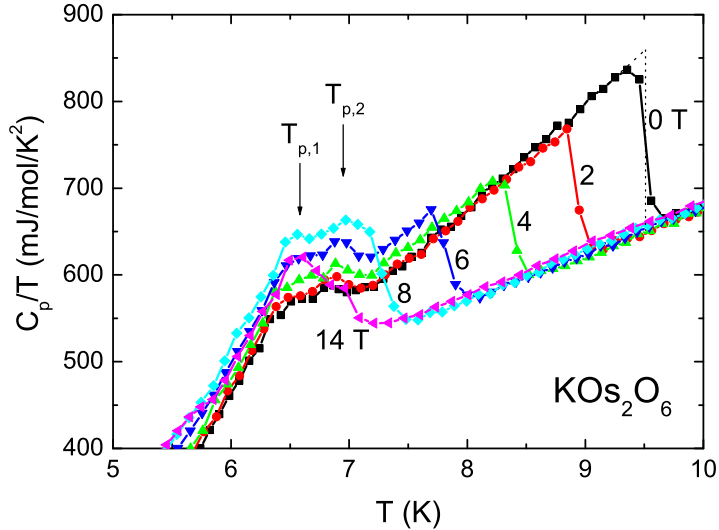


FIG. 3: (Color online) Heat capacity versus temperature of  $\text{KOs}_2\text{O}_6$  for various magnetic fields. The specific heat jump at  $T_c$ ,  $\Delta C_p|_{T_c}/T_c$  is  $204 \text{ mJ}/(\text{mol K}^2)$ , from which the normalized specific heat jump  $\Delta C_p|_{T_c}/(\gamma T_c) = 2.7 \{1.9\}$  is extracted. It is significantly larger than that for the weak-coupling case and corresponds to an electron-phonon coupling constant  $\lambda_{\text{ep}} \approx 1.0 \{1.6\}$ , i.e.  $\text{KOs}_2\text{O}_6$  is a superconductor in the strong-coupling regime. There are two transitions at  $T_{\text{p},1} \approx 6.5 \text{ K}$  and  $T_{\text{p},2} \approx 7 \text{ K}$  that might be associated with K ordering.

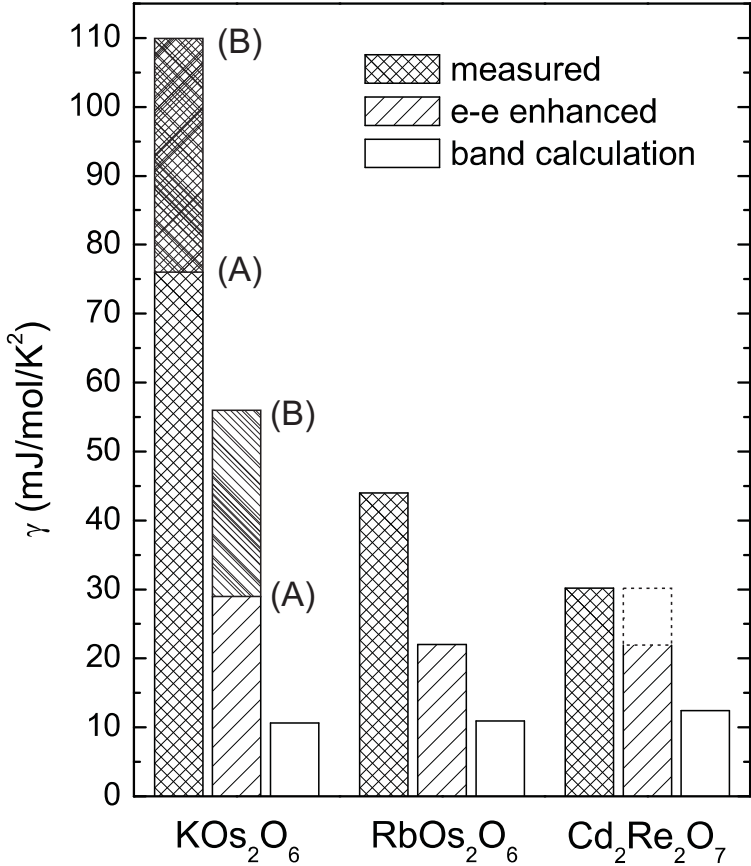


FIG. 4: Comparison of the Sommerfeld coefficients for  $\text{RbOs}_2\text{O}_6$ ,  $\text{KOs}_2\text{O}_6$ , and the weak-coupling  $\alpha$ -pyrochlore superconductor  $\text{Cd}_2\text{Re}_2\text{O}_7$ . Shown are the calculated bare coefficients  $\gamma_b$  in white, the electron-electron enhanced coefficients  $(1 + \lambda_c)\gamma_b$  in hatched, and the measured coefficients  $(1 + \lambda_{\text{ep}})(1 + \lambda_c)\gamma_b$  in cross hatched. The bare band value from DFT calculations in the LDA is rather similar for all three pyrochlores. The electron-phonon coupling  $\lambda_{\text{ep}}$  increases from  $< 0.4$  (weak coupling) for  $\text{Cd}_2\text{Re}_2\text{O}_7$  to 1 for  $\text{RbOs}_2\text{O}_6$  to 1.0 to 1.6 for  $\text{KOs}_2\text{O}_6$ . The two sets of values (A) and (B) for  $\text{KOs}_2\text{O}_6$  correspond to the two choices of extrapolating  $H_{\text{c}2}(T)$  in Fig. 1.

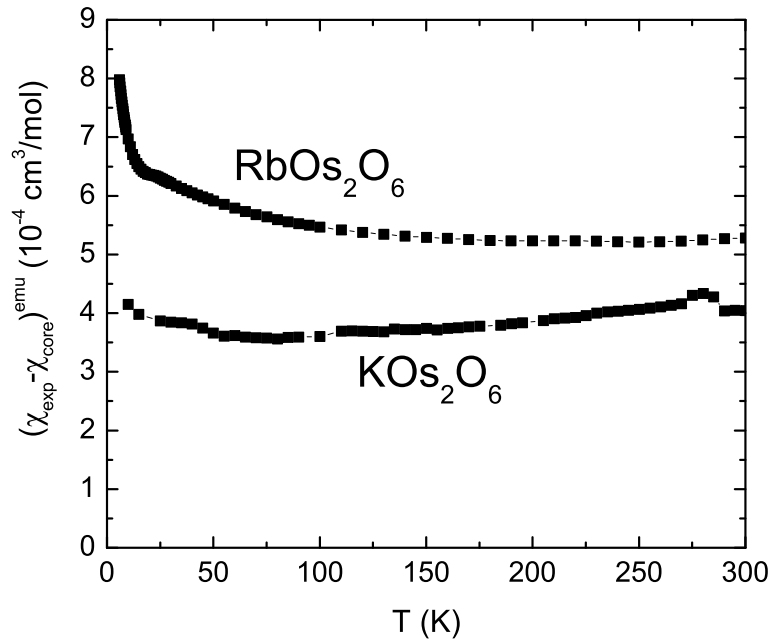


FIG. 5: Magnetic susceptibility of  $\text{KOs}_2\text{O}_6$  and  $\text{RbOs}_2\text{O}_6$  measured at 1 T. The data is corrected for the core diamagnetism ( $+1.22 \cdot 10^{-4} \text{ cm}^3/\text{mol}$  for  $\text{RbOs}_2\text{O}_6$ ,  $+1.15 \cdot 10^{-4} \text{ cm}^3/\text{mol}$  for  $\text{KOs}_2\text{O}_6$ ), resulting in susceptibilities taken at 150 K of  $\chi^{\text{emu}} \approx 3.7 \cdot 10^{-4} \text{ cm}^3/\text{mol}$  for  $\text{KOs}_2\text{O}_6$  and  $\chi^{\text{emu}} \approx 5.3 \cdot 10^{-4} \text{ cm}^3/\text{mol}$  for  $\text{RbOs}_2\text{O}_6$ .

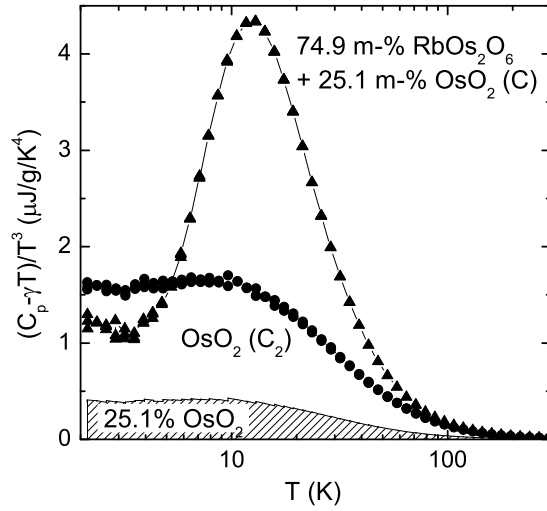


FIG. 6:  $(C_p - \gamma T)/T^3$  versus temperature on a logarithmic scale of a  $\text{RbOs}_2\text{O}_6$  sample with 74.9 mass – %  $\text{RbOs}_2\text{O}_6$  and 25.1 mass – %  $\text{OsO}_2$  and an  $\text{OsO}_2$  sample. It illustrates the significant additional heat capacity present in  $\text{RbOs}_2\text{O}_6$ . The difference between  $C$  and the shaded region is 74.9 % of the intrinsic heat capacity of  $\text{RbOs}_2\text{O}_6$ .

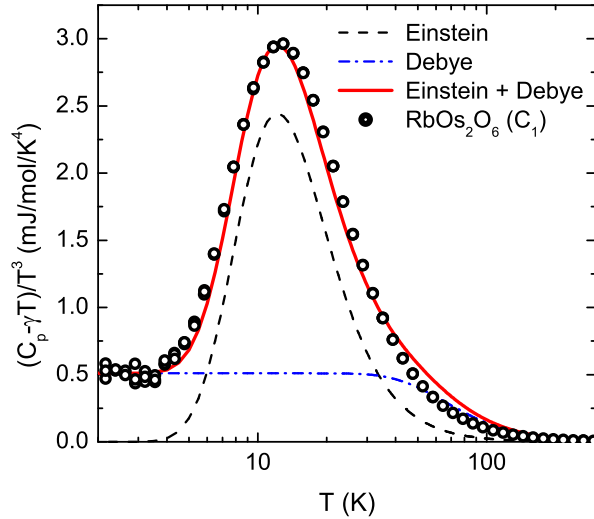


FIG. 7: (Color online) Decomposition of the lattice heat capacity  $(C_p - \gamma T)/T^3$  of  $\text{RbOs}_2\text{O}_6$  into Debye and Einstein-mode components. In such a plot, an Einstein contribution to the heat capacity appears as a bell-shaped feature with a maximum at  $T = T_E/4.93$ .[31] The data are well described by a combined Debye-Einstein model with  $\Theta_D = 325\text{ K}$ ,  $T_E = 60\text{ K}$ , and  $n \approx 0.33 \cdot 9$  modes per f.u.

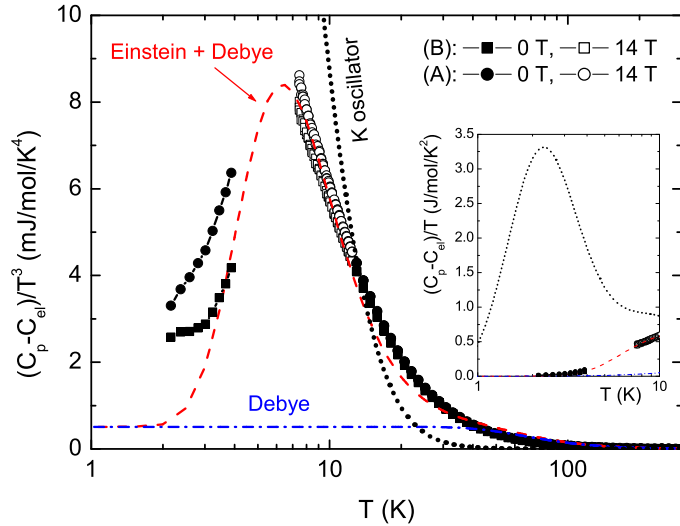


FIG. 8: (Color online)  $(C_p - C_{el})/T^3$  of  $\text{KOs}_2\text{O}_6$  on a logarithmic temperature scale. The dashed line shows a combined Einstein-Debye contribution with  $n = 0.15 \cdot 9$  modes/f.u.,  $T_E = 31$  K, and  $\Theta_D = 325$  K to illustrate a best fit to the data if an Einstein-type contribution is assumed. We use the Debye temperature from  $\text{RbOs}_2\text{O}_6$  (Fig. 7). The dotted line indicates the large lattice contribution expected at low temperatures from a K ion in an anharmonic potential.[32] The absence of such a contribution may indicate a freezing of the rattling motion at  $T_{p,i}$ . (A) and (B) refer to the two extrapolations used to extract  $\gamma$  as described in the main text.

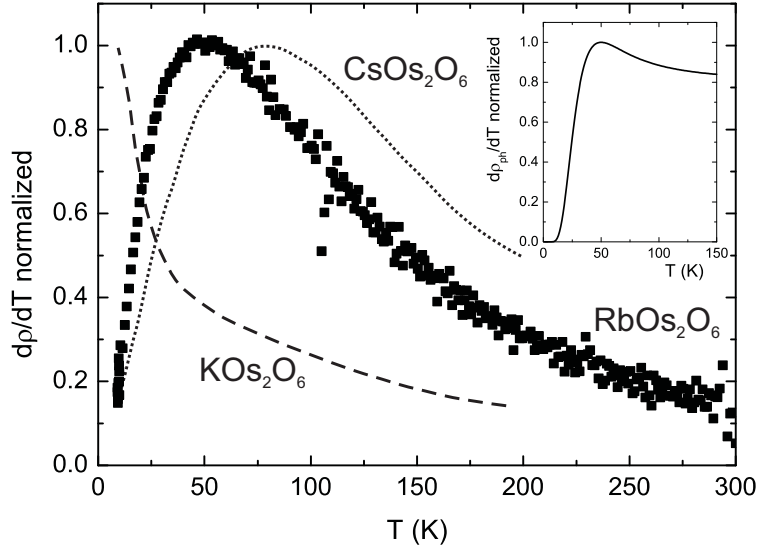


FIG. 9: Temperature derivative of the electrical resistivity  $d\rho/dT$  normalized to the value at its maximum showing the systematic variation of the peak location with the  $A$  ion. The data for  $\text{CsOs}_2\text{O}_6$  (dotted curve) and  $\text{KOs}_2\text{O}_6$  (dashed curve) are taken from Ref. [11] and Ref. [4] respectively. The two curves are smoothed. The inset shows the calculation for a single Einstein phonon.

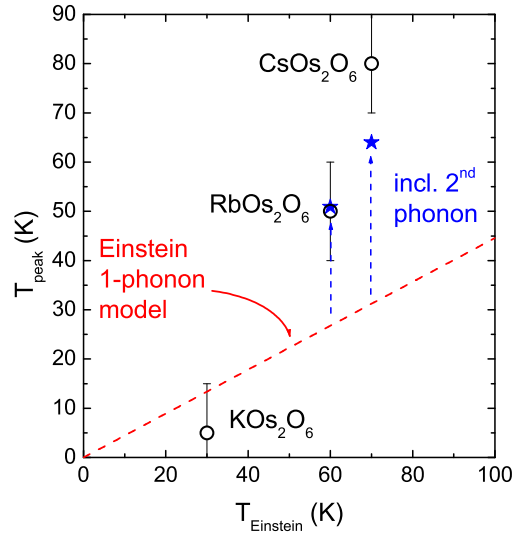


FIG. 10: (Color online) Systematic variation with the  $A$  ion of the maximum in the temperature derivative of the resistivity  $T_{\text{peak}}$  versus the characteristic temperature of the low-energy phonon  $T_{\text{Einstein}}$  extracted from heat capacity measurements. For illustration we show where the maxima are expected to lie according to the solution of the linearized Boltzmann equation for a single phonon by a dashed line.[33] Inclusion of a second phonon by Matthiessen's rule at around 140 K for  $\text{RbOs}_2\text{O}_6$  and around 175 K for  $\text{CsOs}_2\text{O}_6$ [10, 34] moves the peak temperature up towards the measured value shown by the blue stars and arrows.

This figure "CvsHandCrystals.png" is available in "png" format from:

<http://arxiv.org/ps/cond-mat/0602579v1>